(19) Watanabe, M.; Nagaoka, K.; Kanba, M.; Shinohara, I. *Polym. J.* **1982**, *27*, 4191.
(20) Eisenberg, A.; King, M. "Ion-Containing Polymers"; Academic Press: New York, 1977.
(21) Moacanin, J.; Cuddihy, E. F. *J. Polym. Sci., Part C* **1966**, *14*, 313.
(22) Hannon, M. J.; Wissbrum, K. F. *J. Polym. Sci., Polym. Phys. Ed.* **1975**, *13*, 113.
(23) Wetton, R. E.; James, D. B.; Whiting, W. *J. Polym. Sci., Polym. Lett. Ed.* **1976**, *14*, 557.
(24) Sorensen, P. R.; Jacobsen, T. *Electrochim. Acta* **1982**, *27*, 1671.
(25) Williams, M. L.; Landel, R. F.; Ferry, J. D. *J. Am. Chem. Soc.* **1955**, *77*, 3701.
(26) Cohen, M. H.; Turnbull, D. *J. Chem. Phys.* **1959**, *31*, 1164.
(27) Miyamoto, T.; Shibayama, K. *J. Appl. Phys.* **1973**, *44*, 5372.

# Ionic Conductivity of Polymer Complexes Formed by Poly(β-propiolactone) and Lithium Perchlorate

**Masayoshi Watanabe,*[1a] Makiko Togo,[1a] Kohei Sanui,[1a] Naoya Ogata,[1a] Tadahiko Kobayashi,[1b] and Zentaro Ohtaki[1b]**

*Department of Chemistry and Department of Electrical and Electronic Engineering, Sophia University, Kioi-cho, Chiyoda-ku, Tokyo 102, Japan.* *Received April 17, 1984*

ABSTRACT: The correlation between molecular characteristics and electrical conductivity in poly(β-propiolactone)–lithium perchlorate (PPL–$LiClO_4$) complexes was investigated. The complex impedance and direct current measurements on a cell made of the PPL–$LiClO_4$ complex sandwiched between platinum and/or lithium electrodes revealed that the electrical conductivity was due to migration of $Li^+$ with a transference number of nearly unity. It was found that the dissolution of $LiClO_4$ in PPL facilitated the formation of a new crystalline phase with a higher enthalpy of melting than that of pure PPL. The degree of crystallinity decreased with increasing $LiClO_4$ concentration. The temperature dependence of the conductivity showed Arrhenius-type behavior in the low-concentration complex, while it showed WLF-type behavior in the high-concentration complex. The enhancement of conductivity by quenching implied that ion migration in the amorphous region was the main contribution to the ionic conductivity. A maximum conductivity of $3.7 \times 10^{-4}$ S cm$^{-1}$ was observed in the quenched complex at 70 °C.

## Introduction

It is well-known that electrical conduction in ordinary polymers at low electric fields is due to migration of ions originating from ionic impurities in the bulk, absorbed moisture, and decomposition products of polymers.[2-6] The conduction current in these polymers is extremely low, and thus, polymeric materials have been used in electrical fields as insulators or dielectrics. However, a relatively high ionic conductivity was recently reported in ion-containing polymers such as poly(ethylene oxide)- and poly(propylene oxide)–alkali metal salt complexes.[7-10] These findings have stimulated increasing interest in ion-containing polymers with high ionic conductivity because of their potential applications to primary or secondary solid-state batteries, electrochemical displays, and so on.

It was demonstrated by several authors[11-14] that the high ionic conductivity of the polyether complexes could be attributed to ion transport within amorphous regions of the polymers. The segmental mobility of the polyethers with low glass transition temperatures ($T_g \simeq -60$ to $-70$ °C) is very high at ambient temperatures, which contributes to high mobility of ionic carriers. Structural characteristics such as the polar ether oxygen which exists at every three atoms in the polymer backbone, ensure a cooperative interaction of neighboring oxygen atoms to ions by analogy with the macrocyclic polyethers. This interaction seems to contribute to the generation of a large number of ionic carriers. Thus, the polymers which have both a high concentration of highly polar groups and a low $T_g$ are expected to be ionic conductors in the polymer–salt systems.

In an earlier article,[15] we reported that poly(ethylene succinate)–lithium perchlorate (PE-2,4–$LiClO_4$) complexes had a relatively high ionic conductivity comparable to that of poly(ethylene oxide)–lithium salt complexes. $LiClO_4$ was dissolved in the amorphous region of PE-2,4 but did not form a new crystalline phase with the polymer. The conductivity was attributed to an ion transport process in the amorphous region. As a result, the temperature dependence of the conductivity obeyed a Williams–Landel–Ferry(WLF)-type equation. In this study, poly(β-propiolactone) (PPL) which had a similar structure to PE-2,4 was selected as the host polymer to $LiClO_4$. Lithium ion ($Li^+$) conduction in the PPL–$LiClO_4$ complexes was demonstrated by means of complex impedance and direct current (dc) measurements on a cell with platinum and/or lithium electrodes. The correlation between molecular characteristics and the temperature dependence of the conductivity was investigated.

**Table I**
**Characterization of Poly(β-propiolactone)**

| abbrev | $\eta_{sp}/C^a$ (100 cm$^3$ g$^{-1}$) | GPC data $M_n/10^4$ | $M_w/10^4$ | $M_w/M_n$ |
|---|---|---|---|---|
| PPL | 0.43 | 1.90 | 4.76 | 2.50 |

[a] 0.1 g/10 cm$^3$ in chloroform at 30 °C.

## Experimental Section

**A. Materials.** PPL was synthesized by means of ring-opening polymerization at a low temperature with diethylzinc/water as a catalyst.[16]


A *n*-hexane solution containing 0.5 mol % diethylzinc was prepared under a dry nitrogen atmosphere. A 57-cm$^3$ portion of the solution was transferred by a trap-to-trap method into a polymerization tube with a side tube sealed with a rubber cap and was cooled to 0 °C. An equimolar amount of water was added through the side tube by using a microsyringe. The content was sonicated to yield a pale yellow precipitate and was cooled to −30 °C. A 21-g (0.3 mol) quantity of freshly distilled β-propiolactone was

0024-9297/84/2217-2908$01.50/0 

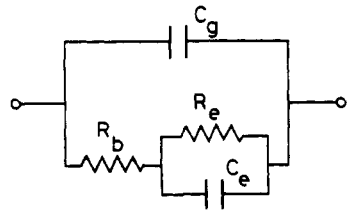


**Figure 1.** Equivalent circuit to interpret complex impedance spectra: $C_g$, geometrical capacity; $R_b$, bulk resistance; $R_e$, electrolyte/electrode interfacial resistance; $C_e$, electrolyte/electrode interfacial capacity.

added to the contents by a trap-to-trap method. The polymerization tube was evacuated, degassed repeatedly, and sealed. Polymerization was carried out at −25 °C for 72 h. The PPL product was purified by reprecipitation using chloroform–ethyl alcohol, followed by washing successively with water and ethyl alcohol. The sample characteristics are summarized in Table I. Average molecular weights were estimated on a gel permeation chromatograph (Waters Associate Inc., 150C) with a RI detector at 100 °C by using *m*-cresol as the carrier solvent. Narrow-distribution polystyrenes were used as elution standards.

**B. Preparation of PPL–$LiClO_4$ Complexes.** A special grade anhydrous $LiClO_4$ (Mitsuwa Kagaku Co.) was dried under a reduced pressure ($10^{-3}$ torr) at 180 °C for 8 h.

The $LiClO_4$ was dissolved directly in PPL at 100 °C under a nitrogen stream to form various concentrations. After the solutions became optically homogeneous, they were cooled to room temperature to yield crystalline complexes which were crushed finely. These procedures were repeated twice in order to achieve a homogeneous dissolution of $LiClO_4$ in PPL. Standard inert-atmosphere techniques were used during the preparation in order to exclude traces of water.

**C. Methods.** The electrical properties were measured on a pressed cylindrical pellet sandwiched between platinum and/or lithium electrodes. Alternating current (ac) measurements were made on the cell with a Hewlett-Packard 4800A vector impedance meter over a frequency range of 5 Hz to 500 kHz. Direct current (dc) measurements were made by applying a constant voltage over the cell and measuring the current with a Keithley 610C electrometer.

Differential scanning calorimetry (DSC) was carried out on a DSC apparatus (Rigaku Denki Co., 8085) at a heating rate of 20 °C $min^{-1}$. X-ray diffraction patterns were measured with an X-ray diffractometer (Rigaku Denki Co., RAD-IIA) by using a Ni-filtered Cu $K_\alpha$ line. Quantitative analysis of lithium was carried out with an atomic absorption spectrophotometer (Dai-ni Seiko Co., SAS-727).

## Results and Discussion

**A. Lithium Ion Conduction in PPL–$LiClO_4$ Complexes.** We assumed that the equivalent circuit shown in Figure 1 can be used to interpret the frequency dependence of the impedance spectra of the present cell system.[15] Definitions of $C_g$, $R_b$, $C_e$, and $R_e$ are cited in the figure caption. Figure 2 shows the typical complex impedance spectra of the cells with platinum electrodes (a) and with lithium electrodes (b). The profile of the spectrum of the platinum electrode cell (a) was an arc having a low-frequency branch, whereas that of the lithium electrode cell (b) was two neighboring arcs. The high-frequency arcs were similar in the spectra of both cells; however, the low-frequency impedance loci were different. Thus, it was suggested that the low-frequency and high-frequency impedance loci corresponded to electrolyte/electrode interfacial impedance and bulk electrolyte impedance, respectively.

These impedance responses can be interpreted simply on the assumption that $C_g \ll C_e$, which is often the case in these electrolyte cell systems. On the basis of this assumption we intended to estimate the values of $C_g$, $R_b$, $C_e$, and $R_e$ and to simulate the impedance spectra. At low

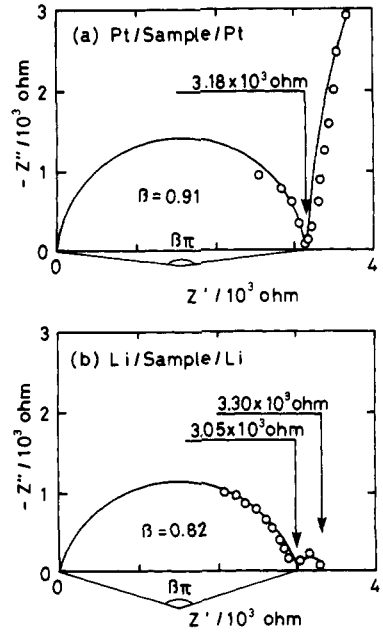


**Figure 2.** Complex impedance spectra at 60 °C for PPL–$LiClO_4$ complex ([$LiClO_4$]/[unit] = 0.1) with the same thickness. Solid lines in the figure are simulated spectra.

frequencies ($\omega \simeq 1/R_eC_e$), $C_g$ is considered to be open. The equivalent circuit of Figure 1 can therefore be reduced by $R_b$ in series with the parallel combination of $R_e$ and $C_e$. The impedance ($Z$) of the reduced equivalent circuit can be written as follows:

$$Z = R_b + \frac{R_e}{1 + i\omega R_eC_e} \qquad (\omega \simeq 1/R_eC_e) \qquad (1)$$

The profile of the impedance spectrum based on eq 1 is an arc centered at $R_b + R_e/2$ on the $Z'$ axis with a radius of $R_e/2$ and corresponds to the interfacial impedance. The values at low- and high-frequency ends of the arc coincide with $R_b + R_e$ and $R_b$, respectively. At high frequencies ($\omega \simeq 1/R_bC_g$), the equivalent circuit of Figure 1 is symbolized by the parallel combination of $R_b$ and $C_g$, and its $Z$, corresponding to the bulk electrolyte impedance, is expressed as follows:

$$Z = \frac{R_b}{1 + i\omega R_bC_g} \qquad (\omega \simeq 1/R_bC_g) \qquad (2)$$

The locus of eq 2 is an arc centered at $R_b/2$ on the $Z'$ axis with a radius of $R_b/2$. However, the centers of the high-frequency arcs in the measured impedance spectra lay apparently below the $Z'$ axis. In order to account for this offset, a phase angle ($\beta$) which measures the deviation of the center of the arc from the $Z'$ axis was introduced, as shown in Figure 2. In this case eq 2 can be rewritten as follows:

$$Z = \frac{R_b}{1 + (i\omega R_bC_g)^\beta} \qquad (\omega \simeq 1/R_bC_g) \qquad (2')$$

According to the Cole–Cole theory, the real ($Z'$) and the imaginary ($Z''$) parts of eq 2′ are written as follows:

$$Z' = \frac{1}{2}R_b\left[1 - \frac{\sinh \beta x}{\cosh \beta x + \cos(\beta\pi/2)}\right] \qquad (3a)$$

$$Z'' = \frac{1}{2}R_b\frac{\sin(\beta\pi/2)}{\cosh \beta x + \cos(\beta\pi/2)} \qquad (3b)$$

where $x = \ln \omega R_bC_g$.

**Table II**
**Parameters To Simulate Complex Impedence Spectra by Using an Equivalent Circuit**

| cell | $R_e/\Omega$ | $C_e/F$ | $R_b/\Omega$ | $C_g/F$ | $\beta$ |
|---|---|---|---|---|---|
| Pt/sample/Pt | $1.7 \times 10^4$ | $1.6 \times 10^{-6}$ | $3.18 \times 10^3$ | $7.0 \times 10^{-11}$ | 0.91 |
| Li/sample/Li | $2.5 \times 10^2$ | $8.8 \times 10^{-7}$ | $3.05 \times 10^3$ | $7.0 \times 10^{-11}$ | 0.82 |

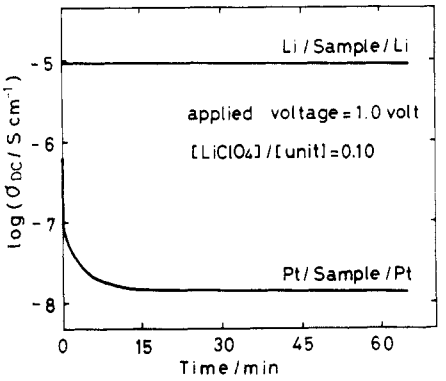


**Figure 3.** Time dependence of apparent dc conductivity at 60 °C for PPL–$LiClO_4$ complex ([$LiClO_4$]/[unit] = 0.1).

By using eq 1 and 2′ and the parameters indicated in Table II, we could simulate the impedance spectra, as shown with the solid line in Figure 2. The simulated lines expressed the measured impedance spectra fairly well. However, the reliability of the $R_e$ and $C_e$ values of the platinum electrode cell is considered to be low compared with that of the other values, because the measured spectrum, expressing the interfacial impedance, is only a high-frequency part of the arc in this frequency range. Thus, as for the $R_e$ values, we could only say that the $R_e$ value in the platinum electrode cell is considerably higher than that in the lithium electrode cell. If the PPL–$LiClO_4$ complexes are assumed to be $Li^+$ conductors, platinum may act as a blocking electrode for the complex. Thus, the charge transfer at the interface between the complex and the electrodes cannot occur. This results in a large $R_e$ value. On the contrary, lithium acts as an activated electrode for the complex which ensures reversible charge transfer ($Li \rightleftarrows Li^+ + e$) at the interface. The $C_e$ values were somewhat larger in the platinum electrode cell. This may be due to the contribution of $Li^+$ polarization at the electrolyte/electrode interface in this cell. The $R_b$ and $C_g$ values in these two cells coincided with each other. However, the $\beta$ value of the lithium electrode cell was somewhat smaller than that of the platinum electrode cell. The precise mechanism of this behavior is still not clear.

Figure 3 shows the time dependence of the apparent dc conductivity calculated from the change in current with time under an applied voltage of 1.0 V. The measurement was carried out on the same samples shown in Figure 2 after the impedance measurement. In the cell with platinum electrodes the conductivity decreased rapidly during the initial 15 min and continued to decrease gradually to reach a value of about $10^{-8}$ S $cm^{-1}$ at 60 min. Since platinum was a blocking electrode for the PPL–$LiClO_4$ complexes, a drop in the effective electric field across the sample occurred because of the formation of a space charge in the vicinity of electrodes. Thus, the conductivity appeared to decrease. On the contrary, the cell with lithium electrodes showed a constant dc conductivity of $10^{-5}$ S $cm^{-1}$, which was higher than that of the platinum electrode cell by 3 orders of magnitude. The constant conductivity agreed with the conductivity calculated from the resistance of $3.30 \times 10^3$ Ω which was assigned to $R_b + R_e$ in Figure 2b. Since $R_b$ is determined by the additional conductance of $Li^+$ and $ClO_4^-$, this agreement suggested that the transference number of $Li^+$ in the PPL–$LiClO_4$ complexes is nearly unity. It was found that the electrode reaction (oxidation and reduction of lithium) and the migration of $Li^+$ in the bulk occurred constantly under a dc voltage in the cell with lithium electrodes. Conduction of $Li^+$ in the PPL–$LiClO_4$ complexes was also confirmed by an electrolysis experiment. When the cell with a lithium anode and a platinum cathode was electrolyzed under an applied dc voltage of 3.0 V, the amount of lithium deposited on the cathode increased in proportion to the electric charge through the cell, as shown in Figure 4. The dashed line in the figure shows the theoretical value according to Faraday's law. The current efficiency was about 75%. However, the experiment contained a certain error. All of the deposited lithium could not be measured because some of lithium was left on the surface of the pellet in contact with the platinum electrode.

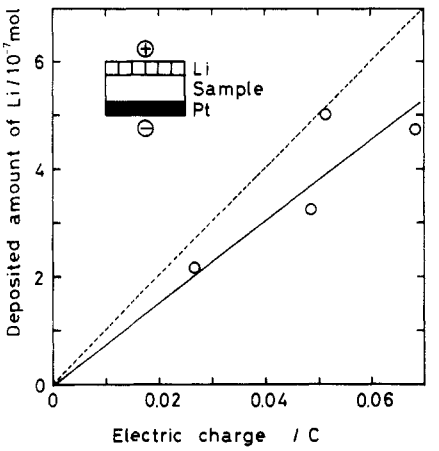


**Figure 4.** Relation between deposited amount of lithium onto platinum cathode and electric charge through the cell.

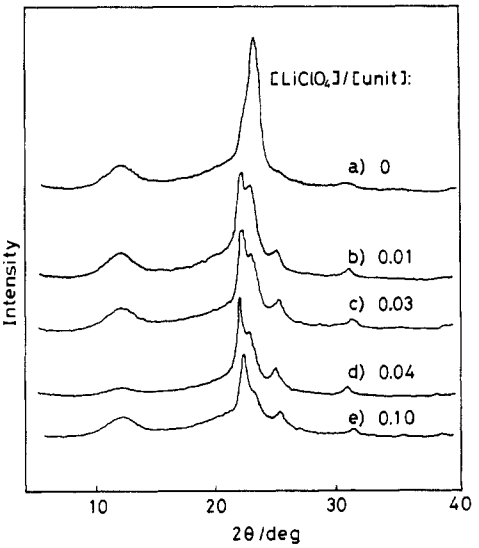


**Figure 5.** X-ray diffraction patterns for PPL and PPL–$LiClO_4$ complexes annealed at 55 °C for 16 h.

From these results it was clear that the PPL–$LiClO_4$ complexes were $Li^+$ conductors.

**B. Correlation between Molecular Characteristics and Temperature Dependence of Conductivity.** Figure 5 shows X-ray diffraction patterns of PPL and PPL–$LiClO_4$ complexes which had been annealed at 55 °C for 16 h before making measurements. PPL showed diffraction peaks at $2\theta = 11.9°$ and 22.9°. In the PPL–$LiClO_4$ complexes new diffraction peaks at $2\theta = 22.0°$, 25.0°, and 31.1°

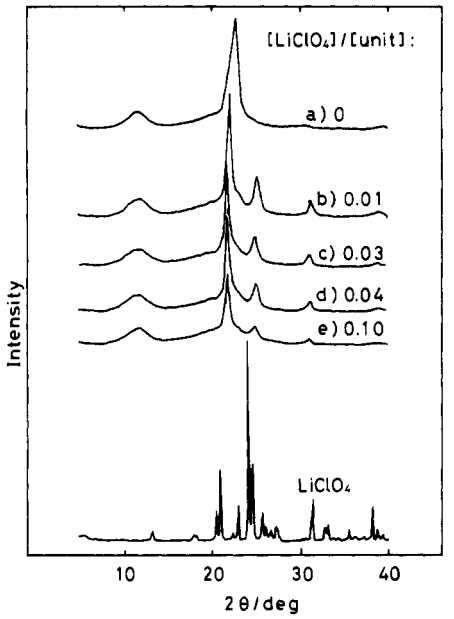


**Figure 6.** X-ray diffraction patterns for $LiClO_4$ and for PPL and PPL–$LiClO_4$ complexes annealed at 55 °C for 72 h.

**Table III**
**Thermal Properties of PPL–$LiClO_4$ Complexes**

| [Li-ClO4]/[unit] | | $T_g$ (zone)/°C | $T_c$, °C | $\Delta H_c$[a]/(cal/g) | $T_m$/°C | $\Delta H_m$[a]/(cal/g) |
|---|---|---|---|---|---|---|
| 0 | 1st | | | | 77 | 33.7 |
| | 2nd | −21 (−24 to −17) | 7 | 5.56 | 74 | 39.3 |
| 0.01 | 1st | | | | 75, 80 | 114.5 |
| | 2nd | −20 (−23 to −17) | 20 | 46.5 | 71, 80 | 85.7 |
| 0.03 | 1st | | | | 73, 79 | 85.8 |
| | 2nd | −16 (−20 to −12) | 28 | 38.5 | 70, 81 | 66.3 |
| 0.04 | 1st | | | | 70 | 96.3 |
| | 2nd | −15 (−18 to −12) | 34 | 36.6 | 66, 76 | 54.6 |
| 0.10 | 1st | | | | 63 | 73.0 |
| | 2nd | −14 (−17 to −13) | | | | |

[a] Phenylazobenzene was used as a standard substance.

appeared in addition to the above peaks. Further annealing altered the X-ray diffraction patterns. In Figure 6 are shown the diffraction patterns for $LiClO_4$ and for PPL and PPL–$LiClO_4$ complexes annealed at 55 °C for 72 h. Annealing for more than 72 h did not change the diffraction patterns, and thus, the PPL–$LiClO_4$ complexes annealed for 72 h seemed to reach equilibrium crystallization. Peaks at $2\theta = 22.9°$ disappeared completely in these PPL–$LiClO_4$ complexes. The fact that the diffraction peaks assignable to $LiClO_4$ did not appear at all implied that $LiClO_4$ in the PPL–$LiClO_4$ complexes dissolved in the host polymer. The intensity of the diffraction peaks decreased with an increase in $LiClO_4$ concentration. Wasai et al.[16] investigated X-ray diffraction patterns of PPL and found that PPL had two crystalline forms, $\alpha$ and $\beta$. The $\alpha$ form had a 2-1 helical structure with a fiber period of 7.02 Å, whereas the $\beta$ form had a planner zigzag structure with a period of 4.82 Å. We tried to assign the new diffraction peaks in the PPL–$LiClO_4$ complexes; however, the peaks could not be attributed completely to the $\alpha$ or $\beta$ form. Thus, the dissolution of $LiClO_4$ seemed to facilitate the formation of a new crystalline phase. However, with an increase in $LiClO_4$ concentration the degree of crystallinity seemed to decrease.

Results of DSC measurements are summarized in Table III. Profiles of DSC curves of the first and second runs are shown in Figures 7 and 8, respectively. The samples used in the first run had been annealed at 55 °C for 72 h

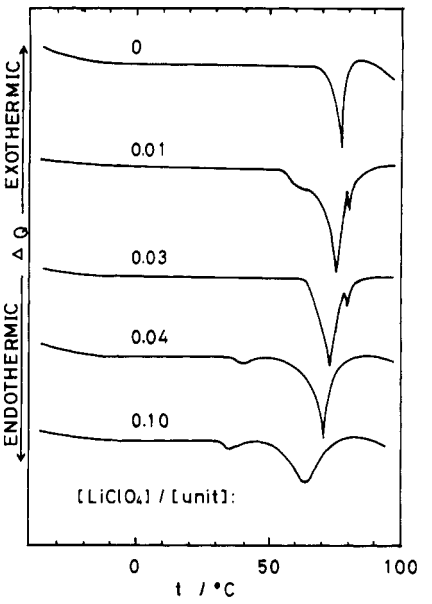


**Figure 7.** Profiles of differential scanning calorimetry curves for PPL and PPL–$LiClO_4$ complexes in the first run. Samples used were previously annealed at 55 °C for 72 h.

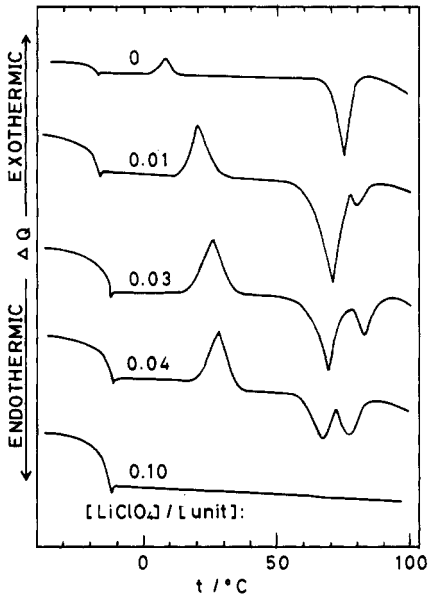


**Figure 8.** Profiles of differential scanning calorimetry curves for PPL and PPL–$LiClO_4$ complexes in the second run. Samples used were quenched from +120 °C to −100 °C.

and corresponded to the samples seen in Figure 6. The second run was carried out after quenching the samples used in the first run with liquid nitrogen from +120 to −100 °C in the DSC apparatus. The enthalpies of crystallization ($\Delta H_c$) and melting ($\Delta H_m$) for the PPL–$LiClO_4$ complexes were represented as a function of unit weight of PPL.

In the first run, only melting points ($T_m$) were clearly determined. PPL showed one endothermic peak at 77 °C with $\Delta H_m = 33.7$ cal/g, whereas the endotherm at $T_m$ for the PPL–$LiClO_4$ complexes of low $LiClO_4$ concentrations split into two peaks and $\Delta H_m$ increased considerably in comparison with the $\Delta H_m$ of PPL. With an increase in $LiClO_4$ concentration, $T_m$ was lowered and $\Delta H_m$ decreased, indicating a decrease in the degree of crystallinity. However, even the complex of $[LiClO_4]/[unit] = 0.1$ showed a larger $\Delta H_m$ than PPL. The increases in $\Delta H_m$'s may be concerned with the formation of a new crystalline phase.

In the second run, PPL showed a $T_g$, a crystallization point ($T_c$) and a $T_m$. The PPL–$LiClO_4$ complexes of

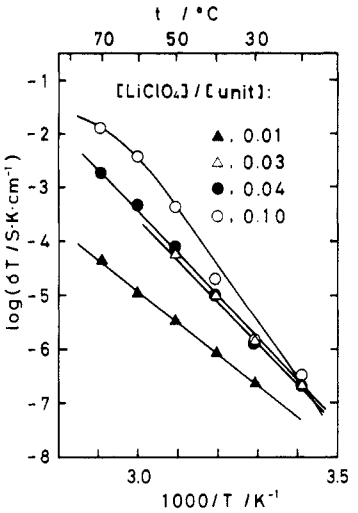


**Figure 9.** Temperature dependence of conductivity for PPL–$LiClO_4$ complexes previously annealed at 55 °C for 72 h.

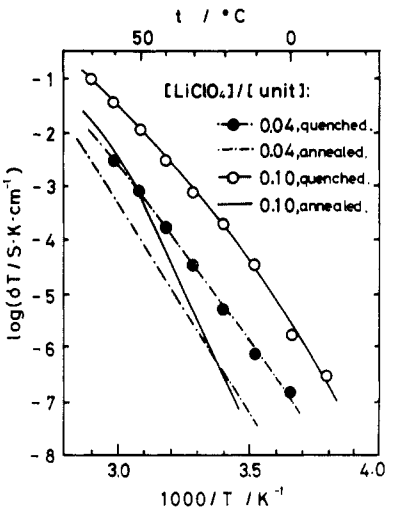


**Figure 10.** Temperature dependence of conductivity of quenched PPL–$LiClO_4$ complexes in comparison with that of annealed complexes.

$[LiClO_4]/[unit]$ = 0.01–0.04 also showed $T_g$, $T_c$, and $T_m$ transitions. The split of $T_m$ became more apparent, compared with that in the first run. Since the complexes were quenched in the second run, the new crystalline phase could not grow sufficiently. The X-ray diffraction patterns of the quenched complexes might correspond to those shown in Figure 5. Thus, two endothermic peaks at $T_m$ seemed to be based on PPL and the complex. A higher one and a lower one may correspond to $T_m$ of PPL and the complex, respectively. An increase in $LiClO_4$ concentration increased $T_g$ and $T_c$, and decreased $\Delta H_c$ and $\Delta H_m$, which indicated that the rate of crystallization was lowered by the dissolution of $LiClO_4$. Consequently, the complex of $[LiClO_4]/[unit]$ = 0.1 did not have any $T_c$ and $T_m$.

Figure 9 shows the temperature dependence of the conductivity ($\sigma$). The $\sigma$ increased with temperature and with $LiClO_4$ concentration. The $\sigma$ reached $3.5 \times 10^{-5}$ S $cm^{-1}$ at 70 °C for the complex of $[LiClO_4]/[unit]$ = 0.1. The temperature dependence for complexes of $[LiClO_4]/[unit]$ = 0.01–0.04 obeyed the following type equation[3,6,17]

$$\sigma = \frac{\nu a^2 q N_0}{kT} \exp\left(-\frac{W/2\epsilon + U}{kT}\right) \qquad (4)$$

where $\nu$ is the vibrational frequency of the trapped ion, $a$ is the jump distance between equilibrium positions, $q$ is the charge of an ionic carrier, $N_0$ is a constant, $k$ is the Boltzmann constant, $W$ is the ionic dissociation energy, $\epsilon$ is the dielectric constant, and $U$ is the potential barrier between equilibrium positions. Equation 4 holds for the hopping conduction of ionic carriers over the potential barrier of $U$ at a low electric field ($E \ll kT/qa$). The ionic carriers are generated from ion pairs which dissociate with the energy of $W$ in a polymer having the dielectric constant of $\epsilon$. The relation between $\log \sigma T$ and $1/T$ for the complex with $[LiClO_4]/[unit]$ = 0.1 was not a straight line function. It is still unclear whether $LiClO_4$ in the complexes is incorporated in the crystalline phase or in the amorpous phase. However, the activation process was dominant for ionic conduction in the low-concentration complexes. With decreasing degree of crystallinity, ionic conduction began to correlate with the segmental mobility in the amorphous region, which led the temperature dependence of $\sigma$ to obey a WLF-type equation.[18]

Figure 10 shows the temperature dependence of $\sigma$ for the quenched complexes in comparison with that for the annealed complexes at 55 °C for 72 h. It should be noted that the quenching of the complex enhanced $\sigma$ by 1–3 orders of magnitude. The $\sigma$ of $3.7 \times 10^{-4}$ S $cm^{-1}$ at 70 °C for the quenched complex of $[LiClO_4]/[unit]$ = 0.1 was comparable to, or higher than, that for the poly(ethylene oxide)–lithium salt complexes. The increase in $\sigma$ with quenching implied that this increase was not caused by an increase in the number of ionic carriers but by ionic mobility.[19] Ion migration in the amorphous phase mainly contributed to the high ionic conductivity. The reduction of activation energy by quenching may be due to decreasing distances between ionic carriers which resulted from an effective decrease in $LiClO_4$ concentration in the amorphous phase.

## References and Notes


(1) (a) Department of Chemistry. (b) Department of Electrical and Electronic Engineering.
(2) Barker, R. E., Jr.; Thomas, C. R. *J. Appl. Phys.* **1964**, *35*, 87.
(3) Barker, R. E., Jr.; Thomas, C. R. *J. Appl. Phys.* **1964**, *35*, 3203.
(4) Barker, R. E., Jr.; Sharbaugh, A. H. *J. Polym. Sic., Part C* **1965**, *C10*, 139.
(5) Saito, S.; Sasabe, H.; Nakajima, T.; Yada, K. *J. Polym. Sci., Part A-2* **1968**, *6*, 1297.
(6) Miyamoto, T.; Shibayama, K. *J. Appl. Phys.* **1973**, *44*, 5372.
(7) Wright, P. V. *Br. Polym. J.* **1975**, *7*, 319.
(8) Armand, M. B.; Chabagno, J. M.; Duclot, M. J. In "Fast Ion Transport in Solids"; Vashishta, P., Mundy, J. N., Shenoy, G. K., Eds.; North-Holland Publishing Co.: New York, 1979; pp 131–136.
(9) Watanabe, M.; Ikeda, J.; Shinohara, I. *Polym. J.* **1983**, *15*, 65.
(10) Watanabe, M.; Ikeda, J.; Shinohara, I. *Polym. J.* **1983**, *15*, 175.
(11) Lee, C. C.; Wright, P. V. *Polymer* **1982**, *23*, 681.
(12) Payne, D. R.; Wright, P. V. *Polymer* **1982**, *23*, 690.
(13) Dupon, R.; Papke, B. L.; Ratner, M. A.; Whitmore, D. H.; Shriver, D. F. *J. Am. Chem. Soc.* **1982**, *104*, 6247.
(14) Killis, A.; Le Nest, J. F.; Charadame, H.; Gangini, A. *Makromol. Chem.* **1982**, *183*, 2835.
(15) Watanabe, M.; Rikukawa, M.; Sanui, K.; Ogata, N.; Kato, H.; Kobayashi, T.; Ohtaki, Z. *Macromolecules* **1984**, *17*, 2902.
(16) Wasai, T.; Saegusa, T.; Furukawa, J. *Kogyo Kagaku Zasshi* **1964**, *67*, 601.
(17) Wada, Y. "Kobunshi no Kotaibussei"; Baifukan: Tokyo, 1971; pp 329–331.
(18) Williams, M. L.; Landel, R. F.; Ferry, J. D. *J. Am. Chem. Soc.* **1955**, *77*, 3701.
(19) Sasabe, H.; Sawamura, K.; Saito, S.; Yoda, K. *Polym. J.* **1971**, *2*, 518.